Technical University of Denmark

DTU

McStas

CAMEA

Pyrolytic Graphite Experimental Results

Author:

J. Larsen

ESS

PAUL SCHERRER INSTITUT PSI

EPFL ÉCOLE POLYTECHNIQUE FÉDÉRALE DE LAUSANNE

Content

1 Introduction 2
2 PG Alignments 2
2.1 Tails 2
2.2 Lorentzian Tails and Mosaicity 3
2.3 Further Investigations on RITA II 3
3 Reflectivity and Transmissions Measurement 5
4 Cooled PG Experiments 7
4.1 Experimental Results from DMC 8
4.2 Experimental Results from RITA II 10
5 Outlook 12

1 Introduction

The ultimate goal of the CAMEA concept is to reach a high analysing efficiency. This can be achieved in two ways. An analyzer crystal with medium mosaicity will scatter neutrons with slightly different energies in different directions. Given a sample which is small enough i.e. geometrically limited resolution, then using several detectors next to each other will produce slightly different energy distributions in the different detectors. With one such analyzer bank it is possible to measure several energies. The second way in the CAMEA concept is, many analyzers are placed behind each other selecting different energies. This report deals with the different aspects of the Pyrolytic Graphite (PG) analyzers for CAMEA. In section 2 of this report we present our finding on aligning such a setup of crystals.

With CAMEA, we make use of the finite mosaicity of the analyzer crystals. The broader the mosaicity of the analyzer, the wider the energy band one can measure. However the reflectivity of the analyzer crystal generally decreases as the mosaicity increases. To be able to optimize the reflectivity/mosaicity for the CAMEA concept we checked the peak reflectivities and the integrated reflectivities of 1mm thick PG sheets with different mosaicities. Putting many analyzer crystals behind each other requires that the transmission of the crystals is high for the energies analysed by the others. PG has negligible absorption and low incoherent scattering. However, it is powder-like in the (***a***,***b***)-plane. Thus, due to the (hkl) scattering where h or k is non-zero PG has a different orientation and energy dependent extinction. To select the optimal energies for CAMEA, we have measured the transmission of PG in different orientations and for different energies. These measurements are presented in section 3 of this report.

PG is a soft material and it has low energy phonon branches in a large q-range that can cause undesirable phonon contamination of the analysed beam. This phonon contamination can degrade the resolution [1] or produce spurions around strong Bragg peaks from the sample. In section 4 of this report we measured the diffraction map of PG at different temperatures and present our first measurement of the energy width of PG(002) as function of temperature. PG is a hexagonal crystal which is a powder in the (***a***,***b***)-plane and a single crystal in the ***c***-direction. The lattice parameters are a=2.46 Å and c=6.71 Å.

2 PG Alignments

For the alignment of the different pieces of graphite the two-axis diffractometer Morpheus at PSI was used. One frame at a time was mounted and rocking curves (rotations of the sample around the vertical axis) recorded for the different blades. The wavelength used was λ = 5.05 Å. The horizontal and vertical orientation of all crystals was recorded with a combination of automated and manual movement of the frame, and small pieces of aluminum foil was inserted to co-align the graphite crystals. Unfortunately this also caused the Silicon wafer to bend, making alignment an iterative process.

The measured orientations were compared with laser optic measurements and it was found to agree within 0.1^{o}. Since optical alignment is cheaper and faster the optical method was generally used afterwards for pre-alignment, with the final alignment achieved on Morpheus.

2.1 Tails

During the Morpheus measurements different tails were observed around the PG(002) reflection (see figure 1). Since Morpheus is a diffractometer it was impossible to determine whether these were phonons, spurions or some crystalline tails, though if it was crystallites it would need to be a systematic variation in both orientation and d-spacing. These tails were afterwards explained in detail using RITA II (see section 2.3).

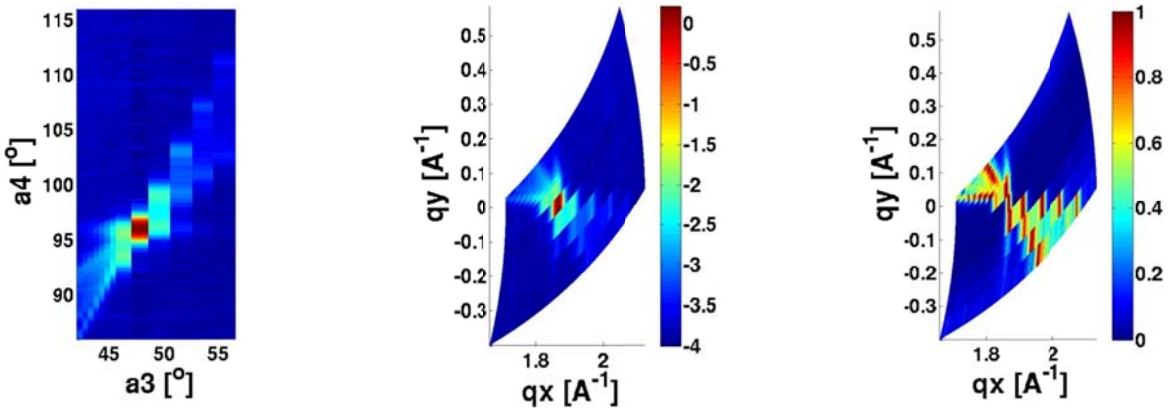

Figure 1: Inelastic stripes around the Bragg peak measured on Morpheus. Left: data in the A3-A4 map in logarithmic scale, middle: data in the q-space (assuming elastic scattering) in logarithmic scale, right: data in the q-space, each A4-scan is normalized to their maximum for the better visibility.

2.2 Lorentzian Tails and Mosaicity

The (002) peak shape of PG is not a perfect Gaussian but has Lorenzian tails. The tails are often 2-3 orders of magnitude below the main peak but they this still limits the performance. However, during the measurements of the different crystals it was seen that a sample dependence exists, so that PG with coarser mosaicity also had stronger Lorentzian tails (see Figure 2), suggesting a structural effect.

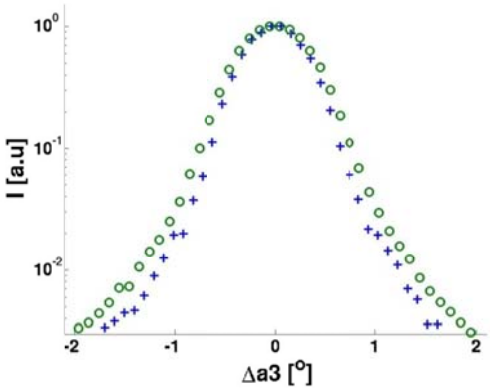

Figure 2: Lorentzian tails of PG (002) measured on Morpheus. The mosaicities are: 0.5° (blue crosses), 0.6° (green circles). The measured intensities are normalized to the peak height.

2.3 Further Investigations on RITA II

To investigate the tails seen on Morpheus, the cold multiplex triple axis spectrometer RITA II at PSI was used. At the beginning we repeated the measurement performed at Morpheus. RITA II was used in diffraction mode without analyzer, thus, the two-dimensional detector gave the intensities at different scattering angles. Figure 3 shows that the signal out of the Bragg peak is also clearly seen on Rita. Then we made a k_f scan in imaging TAS-mode (each analyzer blade analyses the same energy at different A4 values and reflects the neutrons to different places of the 2D PSD) to check whether the signal we get is inelastic.

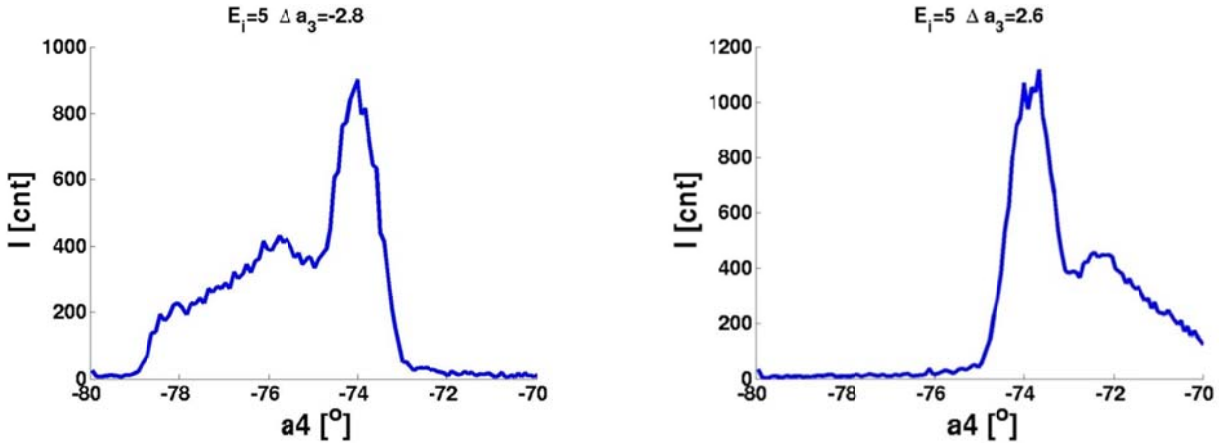

Figure 3: Diffraction measurements at Rita. ΔA3 means the offset from the Bragg position. The high intensity peak at 74° is the tail of the Bragg peak.

In the figure 4 the result is seen in the three-dimensional (***q***,ω) space. The scan shows that at the left side of the Bragg peak the trajectories of the scans at different A4 values are touching the dispersion surface of the graphite phonons. At larger A4 offset the trajectory meshes the surface, while on the other side of the Bragg peak the trajectories go to too low energies, so they do not show any signal.

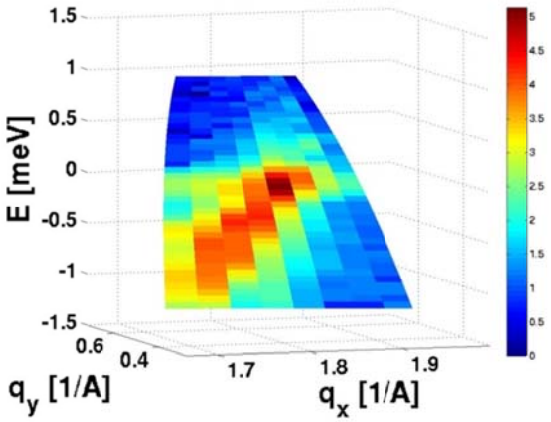

Figure 4: k_f-scan on PG sample near the Bragg peak. The nine different A4-values are given by the nine different analyzer blades of RITA II.

This result proves that the stripes seen in the Morpheus measurement are inelastic signals. For diffraction measurements there is no analyzer, so one sees the integrated intensities of these k_f-scans at different A3/A4 values causing strong signals. Thus, these spurions need further investigations.

We have also checked the mosaicities of the different PG crystals (in TAS imaging mode). In the figure 5 these measurements are seen at 300K, while in the figure 6 the comparisons are seen between the measured rocking curves at 300 K and 5 K. The results show that the Lorenzian tail of the Bragg peak is stronger if the mosaicity of the graphite has higher value, and also show that the Lorentzian tail of the Bragg peak is elastic and temperature independent.

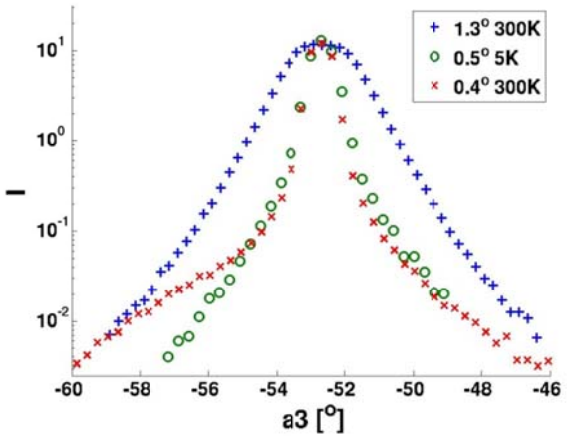

Figure 5: Rocking curves of the different PG analysers. On the left side of the third dataset (mosaicity is 0.4°) shows increasing background because that sample was measured without cryostat.

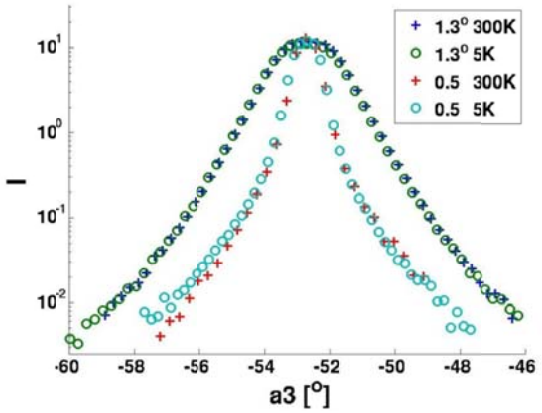

Figure 6: Temperature dependence of the tails of Bragg peaks.

3 Reflectivity and Transmission Measurement

We have made reflectivity measurement on the PG sheets of the prototype at Morpheus. We used a silicon monochromator, a very well collimated incident beam and practically no collimation on the reflected beam. The wavelength was 4.67 Å and the scattering angle was 44.17°.

mosaicity from Xray measurement	0.4	0.5	0.7	1.3
Peak reflectivity	0.70	0.68	0.63	0.48
Relative integrated refelctivity	1.00	1.11	1.30	2.01
fit result: A	0.74	0.70	0.63	0.48
fit result: FWHM	0.65	0.75	1.01	2.06

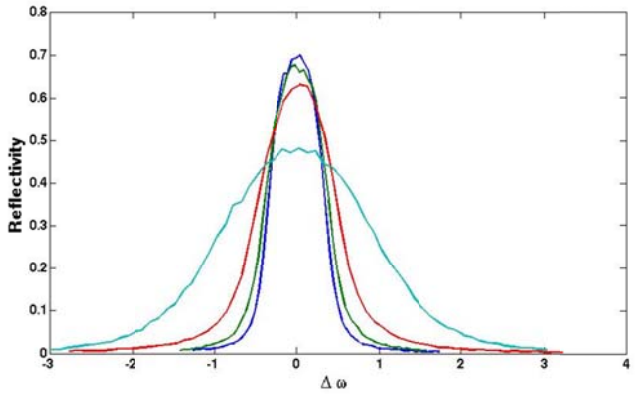

Figure 7: Measured rocking curves of the PG sheets with different mosaicities.

The difference between the measured maximum reflectivity and the fitted value indicates that there is a saturation effect at high reflectivity values.

We made a transmission measurement of the PG with the mosaicity of 0.7° at the MARS instrument at PSI. We used the monitor placed after the sample position, and a 2 mm slit just before the sample. We collected the data in two parts, between 2.6 and 9 meV and between 5.11 and 35 meV. In each chopper setup we rotated the sample between 30° and 75°.

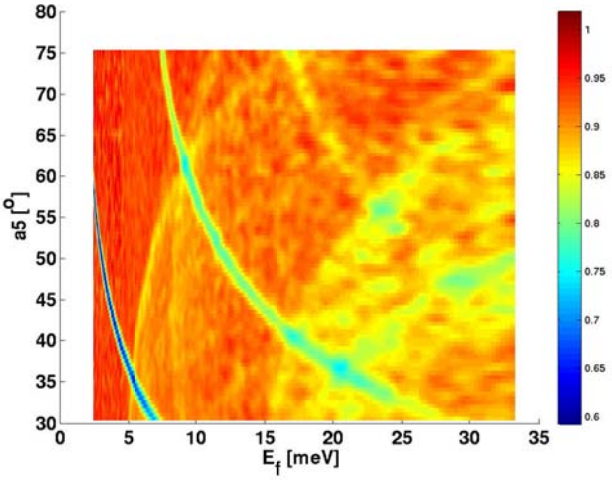

Figure 8: Measured orientation and energy dependent transmission of a 1mm thick PG sheet.

This measurement shows the energy and orientation dependent transmission of the PG. At the designing of the prototype we can calculate the reduction of intensity at a given energy after the analyzers. This helps to define the optimal set of analyzed energies for CAMEA.

4 Cooled PG Experiments

In Refs. [1-3], it was shown that cooling of pyrolytic graphite (PG) analyzer crystals to cryo-temperature greatly improved the signal-to-background ratio (SBR), on the indirect time of flight spectrometers IRIS and OSIRIS at the ISIS facility, see

Figure 9 and Table 1.The SBR ratios quoted in Table 1 were evaluated by first integrating the area around the elastic line ("the signal") from the PG(002) reflection in the raw time spectra. Subsequently the background was found from a similar calculation sufficiently far away from the elastic line ("the background").

For comparison with the geometry of CAMEA, note that the OSIRIS analyzer bank, located 0.7m in front of the detector, consists of 9040 10×1×1 mm^3 PG crystals with a mosaic spread of 0.8^o. The instrument operates with a scattering angle, $2\theta \approx 170$ degrees. The OSIRIS and the IRIS analyzer banks are cooled using three 1.5 W Sumitomo closed cycle refrigerators (CCR's) [2].

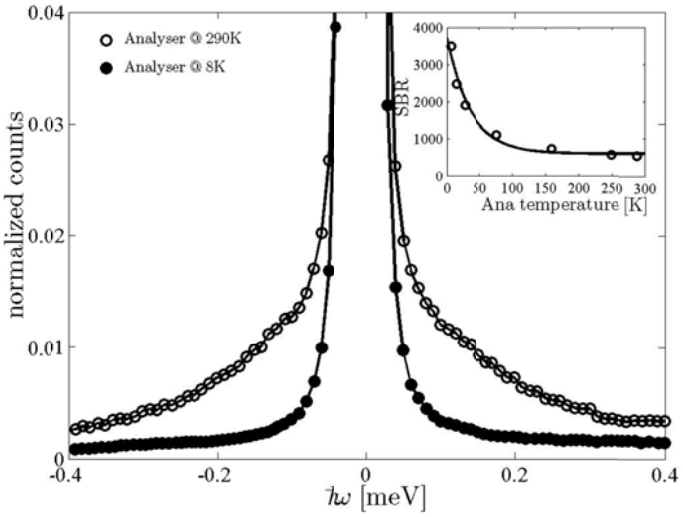

Figure 9: Suppression of the phonon-induced diffuse scattering on the OSIRIS spectrometer. The data was collected with Vanadium at 290K on the sample position. The insert shows the dependence of the SBR on the analyzer temperature. The line shows a fit to an exponential function. Figure adapted from Ref. [1].

	T_{sample} = 300K $T_{analyzer}$ = 300K	T_{sample} = 10K $T_{analszer}$ = 10K
OSIRIS	500:1	3350:1
IRIS	350:1	3250:1

Table 1: Signal-to-background ratios for various combinations of sample (vanadium) and analyzer temperatures. Adapted from Refs. [1,2].

Our previous work, see sections 2 and 3, indicates that PG has strong scattering from phonons (1% close to the Bragg peak). In order to assess if this will be a problem for the proposed CAMEA on ESS, which does not operate as close to the backscattering condition as do OSIRIS and IRIS, we have studied the scattering from a PG sample using the cold powder diffractometer DMC (SINQ, Switzerland). We use the data from this experiment to gain insight into the different contributors to the scattering from PG, and mainly around the PG(002) reflection. The results of this experiment are described in section 4.1.

To evaluate the temperature dependence of the signal-to-background ratio for a non-backscattering instrument, we performed initial inelastic neutron scattering experiments on a standard vanadium sample at the RITA II triple axis spectrometer (SINQ, Switzerland), which was operated with a cooled PG crystal at the analyzer position. The preliminary results of this experiment are described in section 4.2.

4.1 Experimental Results from DMC

DMC has a "Banana" type multi-detector, which consists of 400 BF_3 counters and covers scattering angles from 13^o to 93^o. The instrument is equipped with a focusing monochromator made from 5 PG crystals. A PG filter is installed in the incident neutron beam path. Rotating a single crystal sample on a powder diffraction instrument like DMC yields a reciprocal space map of the horizontal scattering plane integrated over the final neutron energy.

In our experiments the incident neutron wavelength was 2.45 Å. The sample was a single 50x10x1 mm^3 PG crystal of mosaicity 0.5^o. It was mounted in vertical position on a thin Aluminium sheet (thickness ~1mm) and inserted into a cryostat. Subsequently, the sample was rotated through an angular range of 180 degrees and the scattering recorded as a function of sample rotation angle, θ, and scattering angle, 2θ.

We performed measurements at 10K and 290K. The data are shown in figure 10 and 11, respectively, where they are plotted versus Q_x and Q_y. Here Q_x is parallel to the crystallographic c-axis of pyrolytic graphite and Q_y is an in-plane direction. The data have been symmetrized to cover 360 degrees in sample rotation angle, θ, and are shown on a logarithmic color scale (log_{10}) for clarity.

Before turning to the scattering related to phonons in graphite, let us first describe the qualitative features of the remaining data starting with sharp Bragg peaks that can be attributed to PG: (i) The PG(002) reflection is clearly visible at (Qx,Qy)=(2,0) and (-2,0). (ii) Also seen are reflections with (Qx,Qy)=(2,1), (1,1) and (0,1). (iii) Second order reflections are suppressed by the filter and we observe only faint contributions ao (-3,0) and (-1,0). (iv) Further, we observed four peaks of unknown origin around (±3, ±0.73), with intensities similar to the second order PG(002) reflections. (v) Curved lines going through the PG(002) reflections in the A4/2θ direction can be observed at both temperatures. These are due to overloading of the detectors when the intense PG(002) peak is in the reflection condition. (vi) A powder ring is visible at the same scattering angle 2θ as the PG(002) reflection. The intensity of the ring is roughly five orders of magnitude smaller the PG(002) reflection. We believe that this feature comes from powder remaining on the crystal surface from the production or from the process of drilling holes in the PG piece for mounting purposes. (vii) In addition, the maps in Figures 10 and 11 show lines of scattering in the (00l)-direction connecting the Bragg peaks. These lines do not have any detectable temperature dependence. While we don't at present have a clear understanding of the origin of these lines, we speculate that they may be caused by incoherent inelastic scattering from the monochromator followed by Bragg scattering from PG(002).

Finally, we turn to the diffuse scattering contributions around the PG(002) reflections. These are very clearly visible in the 290K data set (Fig. 11), where one also sees the tails of similar diffuse contribution centered at PG(004). At 10K (Fig. 10), however, the part of this diffuse scattering contribution on one side of the PG(002) reflection (e.g. at negative values of Qy with respect to the (Qx,Qy)=(-2,0) reflection) has completely disappeared while the part on the opposite side (at positive values of Qy with respect to the (Qx,Qy)=(-2,0) reflection) still carries spectral weight. If the diffuse scattering is due to phonons, we would associate the former with neutron energy gain processes, which are suppressed to zero at low temperature due to the Bose occupation factor in the phonon cross-section, and the latter with neutron energy loss processes, which are suppressed too, but not fully. Figures 12 and 13 illustrate how the intensity suppression of the diffuse scattering is anisotropic in angular (and therefore in momentum) space.

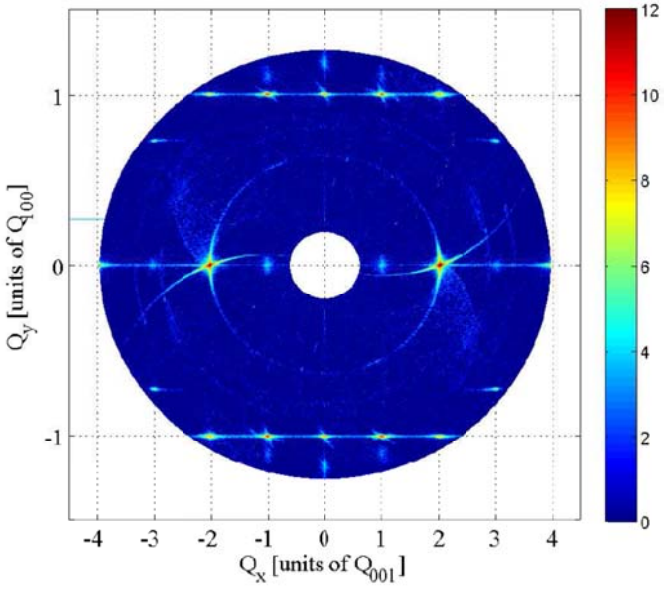

Figure 10: Reciprocal map of PG at 10K. The color scale is logarithmic (log_{10}).

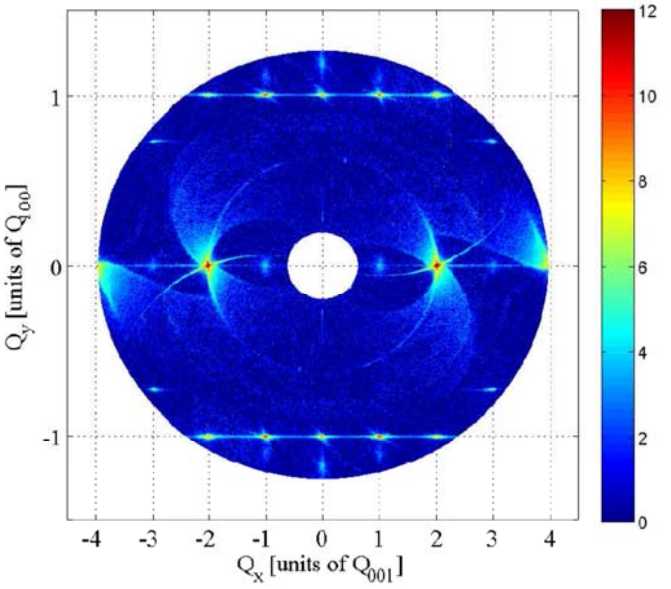

Figure 11: Reciprocal map of PG at 290K. The color scale is logarithmic (log_{10}).

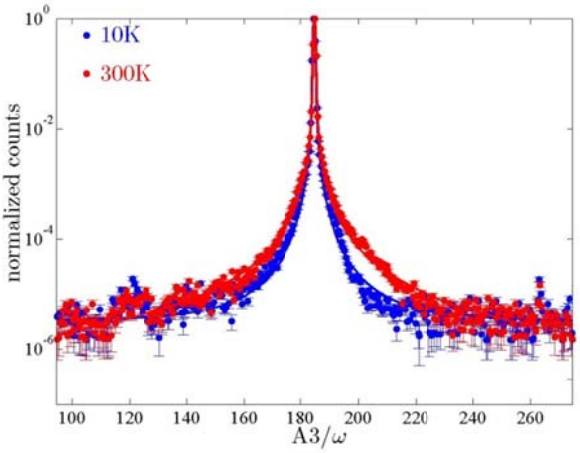

Figure 12: Constant-A4 scans at 10 K and 290 K, integrated over +/-1° around PG(002). Towards higher angles significantly more scattering is observed at 290K.

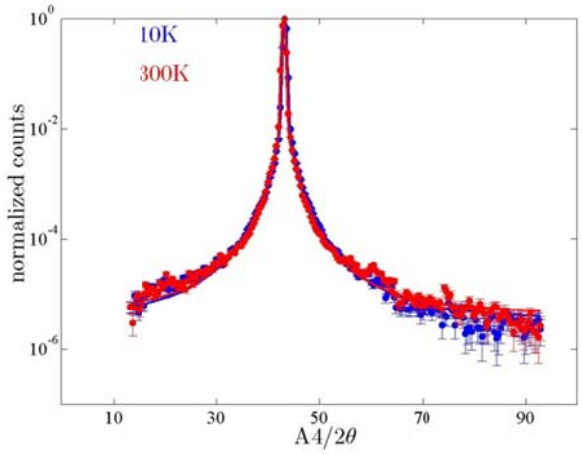

Figure 13: Constant-A3 scans at 10 K and 290 K, integrated over +/-1° around PG(002). Almost no difference is observed.

To prove that the observed diffuse scattering is indeed due to phonons, we performed McStas simulations. DMC was modelled using the built-in McStas instrument PSI_DMC (version: May 7th 2008). At present a dedicated McStas component for phonons in pyrolytic graphite does not exist. Instead we used the Phonon_simple component, which

models acoustic phonons in FCC crystals and takes (among other parameters) temperature and the velocity of sound as entries. Since graphite is hexagonal, such a model will clearly not give an exhaustive account of all the observed scattering in PG (Figs. 10 and 11). However, for our purposes a qualitative comparison is sufficient. We chose a lattice spacing of a_{FCC}=6.71 Å, corresponding to the c-axis lattice constant of PG, and a velocity of sound c_{FCC}≈26 meV Å, which is a reasonable value for phonons travelling along the c-axis. The results of our simulations are shown in Figure 14.

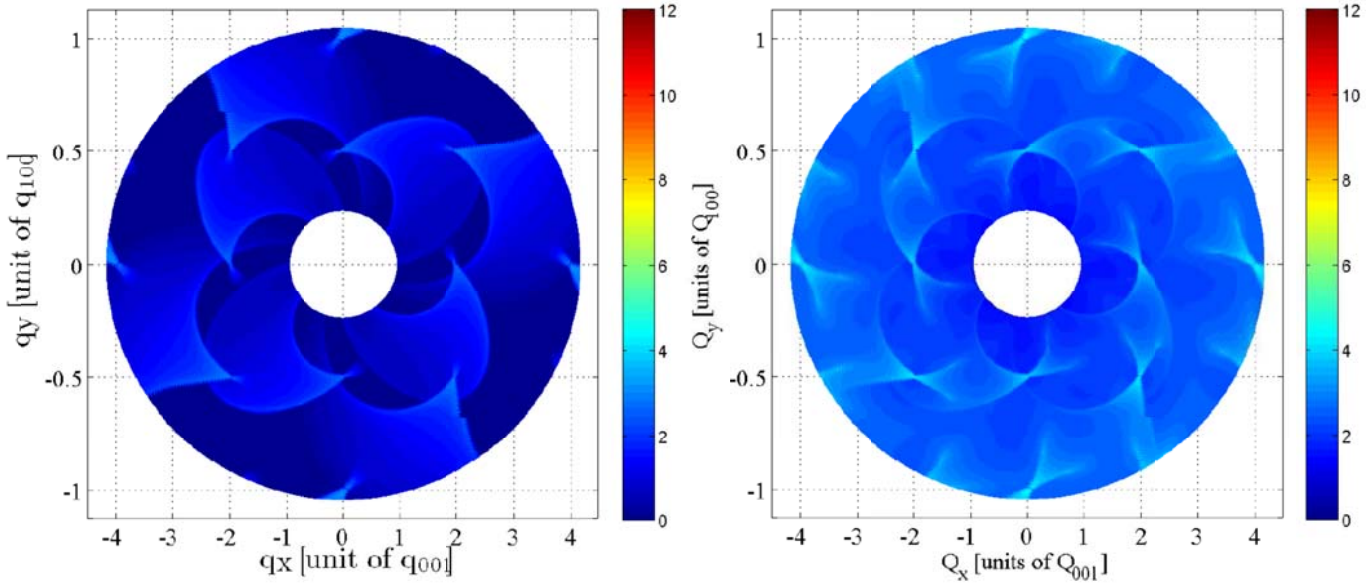

Figure 14: McStas simulations of the scattering from an FCC crystal at 10K (left) and 290K (right). The lattice constant and phonon velocity of sound have been set to the c-axis lattice parameter of PG and the phonon velocity of sound for phonons propagating along c, respectively.

Given that the FCC model does not include elastic scattering at all, there are no Bragg peaks in the maps. Further, we re-emphasize that the model uses an incorrect crystal structure for PG. We therefore limit ourselves to looking at the scattering in the immediate vicinity of (Qx,Qy)=(-2,0).

At 290K the diffuse phonon tails extending from (-2,0) are roughly equally intense at positive and negative values of Qy. By contrast, at 10K, there is a pronounced asymmetry, with the diffuse intensity at negative Qy being suppressed more strongly than the diffuse intensity at positive Qx. Even with the significant limitations of the McStas model for the sample, a comparison between figures 10, 11 and 14 clearly shows that the observed diffuse scattering is due to phonons, and strongly suggests that a McStas simulation using a sample that more accurately reflects the structure of PG will successfully capture all the diffuse intensity in the data maps.

4.2 Experimental Results from RITA II

The aim of this experiment was to measure the energy width and any possible tails directly, by taking data similar to those shown in Figure 9. The low background and large volume of its detector tank makes RITA II ideally suited to this experiment. The analyzer of the triple axis spectrometer RITA II was modified from a 9 blade multiplexed PG analyzer to a single cooled PG blade analyzer mounted inside a CTI cryo device. The CTI was mounted directly on the existing analyzer motor and was fully rotatable, see figure 15. To avoid background from the surrounding instruments and guides

boron enriched plastic blocks were used to shield the front of the setup, see figure 16. For practical reasons the blocks limit the rotation of the CTI, meaning that any optimization of this motor was done prior to the shielding.

The detector of the RITA II instrument is a position sensitive detector (PSD). In front of the detector there is a collimator normally used to avoid cross talk between the 9 blades of the multiplexed analyzer. This collimator is seen just behind the CTI in figure 15 and was kept in our setup, where it serves to minimize background. The total distance between the analyzer and the PSD was roughly 350 mm.

To emulate the experiments at IRIS and OSIRIS as closely as possible, we also used a vanadium sample, which was mounted inside a standard cryostat on the sample position of RITA II. We chose a fixed $k_f = 1.57$ Å^{-1} corresponding to $E_f =$ 5 meV. This is a commonly used energy in cold-neutron triple axis experiments due to the possibility of cleaning away higher-order contamination of the scattered beam using a cooled Be-filter. In our experiment we also used such a filter, placed directly before the entrance into the analyzer tank (the trumpet visible on the left in Figure 15 is where the beam enters the analyzer tank after having passed through the Be filter). The incoming energy was tuned by a PG monochromator and collimated by an 80' collimator. Finally the doors of the RITA II analyzer tank were partially closed and the small opening needed for the CTI tubes and wires was covered with cadmium. The PG analyzer blade, inside the CTI, was mounted on an aluminum plate which was 1mm thick. For this experiment we chose a 50x10x1 mm^3 PG piece of mosaicity 0.5^o, which was thoroughly cleaned before it was inserted in the CTI.

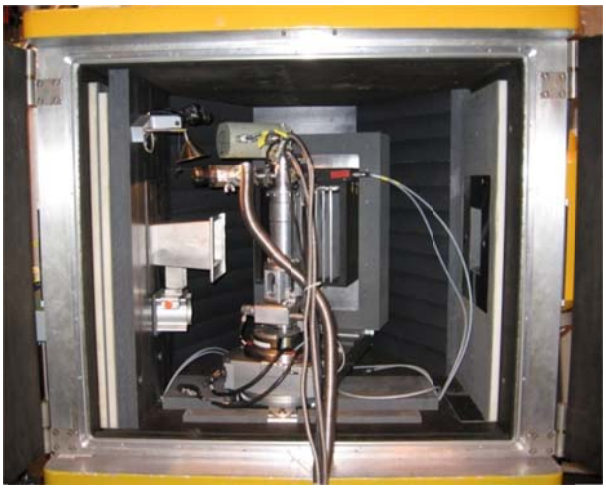

Figure 15: A sideways view into the detector tank of RITA II. On this picture the doors are open. The CTI was mounted on the analyzer motor with a custom-made adapter which brings the PG blade inside the CTI into the right height relative to the neutron beam.

Figure 16: The final shielding of the detector tank, (before closing the doors of the analyzer housing as much as possible) leaving only a necessary hole for the CTI tubes and wires.

Unfortunately, the outcome of the experiment was severely limited due to the unscheduled 2½ week shutdown of SINQ. We were able to set up and acquire only two complete datasets - both with the vanadium sample at 10K. We performed constant two Q-scans between -1 meV and +1 meV in 41 points at an analyzer temperature of 10 K and 290 K (See Figures 17 and 18). We observe that the width of the elastic peak is slightly larger at 290 K than at 10 K, see figure 8. Using a simple fit to a single Gaussian peak profile we find FWHM(T=290 K) = (0.1945±0.0016) meV and FWHM(T=10 K) = (0.1700±0.0021) meV.

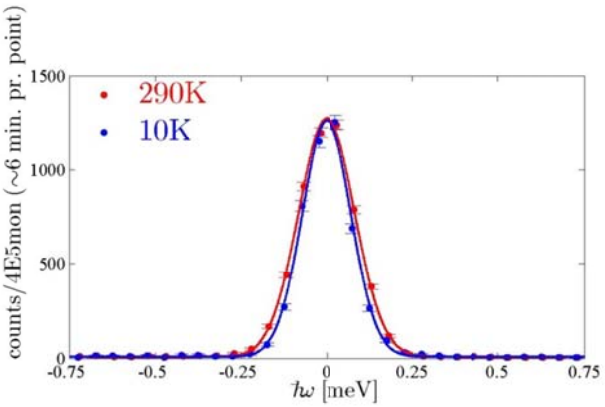

Figure 17: The constant-Q scans of the elastic line from vanadium. The blue and red lines represent fits at 10K and 300K, respectively, as described in the main text.

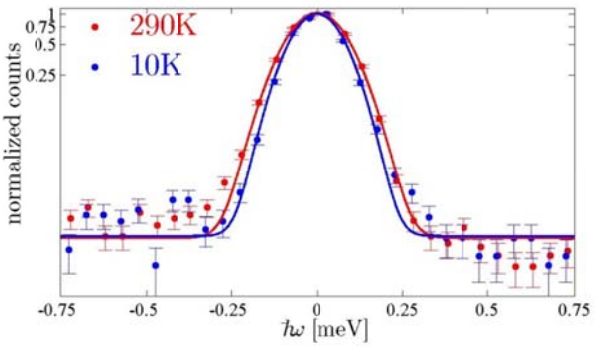

Figure 18: The constant-Q scans normalized to their maximum shown on a logarithmic scale. If any tails are present on either side of the main peak, they are generally easily identified on this scale.

No clear tails/shoulders are observed on either flank of the main peak, see figure 17 (or 18 on a logarithmic scale), indicating only very little contamination from thermal diffuse scattering at the selected value of E_f and with the high-quality 0.5° mosaicity PG piece chosen. A more complicated peak profile consisting of one Gaussian, describing the main peak, plus one Lorentzian, describing any tails, was tried. However, this did not produce stable fits.

5 Outlook

Our original plan for the RITA-II experiments included studying the temperature dependence of the thermal diffuse scattering at different values of A4 and E_f as well as several values of the PG mosaicity. This was not possible due to the unscheduled shutdown mentioned above. Our results are therefore preliminary and will be followed by another test experiment in May 2014. The results of this experiment will feed into the eventual decision process regarding whether to cool the CAMEA analyzers or not.

[1] C.J. Carlile and M.A. Adams, *The design of the IRIS inelastic neutron spectrometer and improvements to its analysers*, Physica B, 182, 431-440 (1992)
[2] M.T.F. Telling et al., *Performance of the cooled pyrolytic graphite analyser bank on the OSIRIS spectrometer at ISIS*, ISIS facility reports (2004)
[3] M.T.F. Telling and K. H. Andersen, *Spectroscopic characteristics of the OSIRIS near-backscattering crystal analyser spectrometer on the ISIS pulsed neutron source*, Phys. Chem. Chem. Phys., 7, 1255-1261 (2005)